Decoupling Surface Topography from Gravitational Acceleration in Cryogenic Pool Boiling

Mohammad S. Reza[1,3], Philip Ignatoff [1,3], Jimmy Almacddissi[1], Jason Hartwig[2]

J. N. Chung[1], Youngsup Song[1*]

[1]Department of Mechanical and Aerospace Engineering, University of Florida, Gainesville, FL, 32611, USA

[2]NASA Glenn Research Center, Cleveland, OH, 44135, USA

Abstract

Boiling heat transfer is governed by a complex interplay between surface conditions and gravitational acceleration. To isolate the sole effects of gravity, we investigated the pool boiling characteristics of liquid nitrogen on atomically smooth silicon dioxide (SiO_2) surfaces under terrestrial (1-g) and reduced gravity (0 ± 0.02 g) conditions achieved via parabolic flight. Our results quantify a drastic reduction in the critical heat flux (CHF) in reduced gravity, decreasing from 16.15 W/cm^2 at 1-g to $5-6$ W/cm^2 at μ-g due to the suppression of buoyancy. Conversely, we observed a distinct increase in the heat transfer coefficient (HTC) in the reduced gravity condition prior to CHF. By utilizing a surface with a maximum peak-to-valley height of ≈ 36.7 nm and low contact angle hysteresis ($< 10°$), we confirm this HTC enhancement is an intrinsic response to the gravitational environment, decoupled from surface-defect-induced nucleation. These findings demonstrate that the influence of surface topography is significantly more

prominent in reduced gravity than in terrestrial conditions, providing a critical baseline for rationalizing the design of cryogenic thermal management systems in space and quantum applications.

Keywords: Parabolic Flight, Critical Heat Flux, Heat Transfer Coefficient, Cryogenic Thermal Management

[*] *Corresponding authors:* Y.S (song@mae.ufl.edu)

[3] *These authors contributed equally*

Introduction

Boiling heat transfer, particularly with cryogenic liquids, is critical for advanced space and quantum computing technologies[1]. From the high-performance thermal management of space electronics and communication payloads[2], to the long-term storage of cryogenic propellants and reliable two-phase microfluidics for orbital laboratories[3], these systems demand precise thermal control harnessing boiling under strict mass and volume constraints. The performance of these boiling systems is defined by three key parameters: the onset of nucleate boiling (ONB) superheat, which defines the point where the first sustained bubble appears, the heat transfer coefficient (HTC), which quantifies the heat transfer efficiency, and the critical heat flux (CHF), which represents the maximum heat flux before the boiling crisis[4]. It is well understood that these parameters are governed by a complex interplay between gravitational acceleration[5] and surface characteristics, e.g., topography[6], wettability[7], and chemical composition[5].

While a significant body of microgravity boiling research has utilized simulant fluids such as FC-72 and HFE-7000 due to their favorable safety profiles and low boiling points[1,8–11], these fluids often exhibit thermophysical property ratios, e.g., liquid-to-vapor density and surface tension, that differ fundamentally from those of cryogenic liquids. Consequently, findings from simulant-based studies may not always be directly transferable to the design of cryogenic thermal management systems required for space propulsion or quantum applications. In this work, we purposefully focus our investigation on the pool boiling of liquid nitrogen (LN_2) on an atomically smooth surface. This targeted scope allows us to establish a physically relevant reference standard that accounts for the unique thermophysical characteristics of cryogens in reduced gravity, effectively filling a critical gap between simulant-based models and the operational requirements of cryogenic flight hardware.

Under Earth-normal gravity (1-g), buoyancy forces dominate, driving rapid bubble departure and effective vapor removal from the heated surface[5,12]. In contrast, reduced gravity (μ-g) suppresses buoyancy, leading to extended bubble residence times, lower bubble departure frequencies, and increased bubble coalescence[1]. While the distinct roles of gravity and surface morphology are individually recognized, a fundamental gap remains in understanding their decoupled effects.

Literature data suggests that surface conditions, e.g., microstructures or defects, can mitigate or augment the effects of reduced gravity. Previous reduced-gravity pool boiling studies (summarized in Supplementary Table 1) have relied largely on metallic surfaces[1,9,13–16], which consistently report a 40-60% reduction in CHF in microgravity relative to terrestrial conditions, with some cases extending up to 80-90% depending on fluid and surface characteristics. These metallic baselines, however, exhibit wide variances in HTC and ONB because their performance is dictated by uncontrolled imperfections like polishing scratches or micro-cavities rather than intrinsic fluid-gravity interactions. More recent efforts have utilized engineered coatings or micro-structured heaters to explore gravity-dependent boiling. These studies, however, typically focus on performance mitigation, e.g., restoring CHF to terrestrial levels, rather than fundamental decoupling[17–19]. Consequently, the thermophysical response of the fluid remains conflated with the specific morphology of the engineered surface. A rigorous baseline dataset that primarily captures the influence of gravity while minimizing topographical effects on a well-defined, ultra-smooth interface is currently lacking. This absence of an atomically smooth, chemically homogeneous baseline compromises the ability to accurately evaluate engineered surfaces and creates a bottleneck in the rational design of space thermal systems.

In this work, we address this unresolved gap by decoupling the effects of gravitational acceleration from surface topography. We harnessed a microfabricated platinum heater deposited directly onto an ultra-smooth silicon dioxide (SiO_2) substrate to characterize the pool boiling of liquid nitrogen (LN_2). This interface, characterized by a maximum peak-to-valley height of only ≈ 36.7 nm and low contact angle hysteresis ($< 10°$), effectively eliminates surface-induced nucleation variables. By removing surface roughness as a variable, we provide a near-ideal control surface to establish the essential reference standard needed to quantify the isolated effects of gravitational acceleration on cryogenic boiling.

Methods

Heater preparation

To ensure an atomically smooth boiling surface, we utilized a prime-grade silicon substrate polished via chemical mechanical planarization. A thin-film platinum micro-heater was fabricated directly on the backside of the oxidized silicon wafer. This backside configuration preserves the pristine topography of the front-facing test surface and eliminates contamination risks associated with conventional soldering or thermal interface materials. The heater was patterned using a standard lift-off process involving photolithography and metal deposition. Complete fabrication details are provided in the Supplementary Note 1 and Supplementary Figure 1. Prior to each boiling experiment, the test surfaces underwent argon plasma cleaning to ensure a pristine, contaminant-free interface[20].

Boiling surface characterization

To ensure that the boiling measurements are driven purely by gravitational acceleration, we rigorously characterized the roughness and wettability of our SiO_2 interface. Figure 1a presents a 5 μm × 5 μm atomic force microscopy (AFM) scan of the boiling surface taken after the experimental campaign. The topography confirms a uniform nanoscale smoothness with a maximum peak-to-valley height of ≈ 36.7 nm. Measurements taken at multiple locations yielded consistent roughness values, verifying the spatial uniformity of the test surface (see Supplementary Figure 2). Comparison with pre-test characterization indicates that while a nominal increase in roughness occurred after the boiling experiments, the interface remained atomically smooth. To contextualize this roughness, we estimated the theoretical wall superheat required for the onset of nucleate boiling (ΔT_{ONB}) using the Young-Laplace and Clausius-Clapeyron relations: $\Delta T_{\mathrm{ONB}} = \frac{2\sigma T_{\mathrm{sat}}}{r_{\mathrm{c}}\rho_{\mathrm{v}}h_{\mathrm{fg}}}$, where σ, T_{sat}, ρ_{v}, and h_{fg} are the surface tension, saturation temperature, vapor density, and latent heat of vaporization, respectively[21]. For LN_2 at atmospheric pressure, a cavity radius (r_{c}) of 30 nm corresponds to a required superheat of approximately 50 K. As shown by Hsu[21], only cavities within a finite size range become active, and predictions based on a single cavity size can deviate from experimental ONB due to thermal boundary layer effects and surface heterogeneity. This order-of-magnitude discrepancy remains a central question in the boiling community, with leading hypotheses suggesting that thermal boundary layer-induced reductions in the nucleation energy barrier or nanoscopic gaseous embryos trapped at contamination sites may govern the actual onset[22,23]. Irrespective of the specific mechanism resolving this discrepancy, the measured surface feature sizes are substantially smaller than the critical scales required to influence nucleation in LN_2. This confirms that the influence of topography on boiling incipience is effectively negligible, ensuring the surface is sufficiently smooth to allow the effects of gravitational acceleration with minimal interference from topographical surface features.

Surface uniformity was further validated via dynamic and static contact angle measurements using deionized water under ambient conditions. While the working fluid is liquid nitrogen (LN_2), direct contact angle measurement with LN_2 is experimentally challenging due to its cryogenic temperature and rapid evaporation. Moreover, LN_2 exhibits near-complete wetting on SiO_2, making it insensitive to subtle surface heterogeneity. Therefore, water contact angle measurements are used as a standard proxy to assess surface cleanliness, chemical homogeneity, and wettability consistency. The static contact angle of water on the SiO_2 surface, measured at five spatially distributed locations, was $18.4° \pm 1.2°$ (mean $\pm$ standard deviation, $n = 5$) (Supplementary Figure 3). This chemical homogeneity, combined with the nanoscale smoothness verified by AFM (Figure 1a), ensures that the surface remains a consistent baseline across repeated experiments. Further, Figure 1b shows a water droplet sliding down on the surface at a tilt angle of 26.5°, exhibiting advancing and receding angles of 20.2° and 10.9°, respectively. The low contact angle hysteresis (<10°) indicates a defect-minimized surface with high chemical homogeneity. Collectively, the nanoscale smoothness and chemical uniformity eliminate localized nucleation sites, establishing this surface as an ideal, defect-minimized baseline for isolating the gravity effects.

Pool boiling experiments

Pool boiling experiments were conducted under terrestrial (1-g) conditions on the ground and subsequently under reduced gravity (μ-g) conditions aboard a parabolic flight. The experimental setup is shown schematically in Figure 2. An insulated Stainless Steel 304 (SS 304) dewar (manufactured by Technifab, Inc.) served as the pool boiling chamber. The pool dewar has an 85 L capacity and is rated to a maximum pressure of 90 PSIG (621 kPa). The heater sample was horizontally mounted at the base of the chamber and fully immersed in LN_2. The heater assembly was configured such that only the front-side boiling surface was exposed to liquid nitrogen. The backside heater pattern, thermocouple junctions, and electrical connections were insulated to prevent direct contact with the liquid, ensuring that the temperature sensors measured the substrate temperature through the solid conduction path rather than being directly influenced by the cryogenic fluid. Instrumentation included two K-type thermocouples (TC_1 and TC_2) attached directly to the backside of the silicon substrate, centered within the heater footprint, using RTV silicone epoxy (Permatex). These sensors measured the substrate base temperature at a depth of 501 μm from the boiling interface. Data were acquired via an NI-9211 module at an effective sampling rate of $\approx 1.4\,\text{Hz}$. The temperature used in the analysis was taken as the average of the TC_1 and TC_2 readings, as the two signals remained in close spatial agreement (typically within ±0.2 K) throughout the experiments. This sampling rate was sufficient to resolve the boiling curve during the ≈ 20 s microgravity windows, as the high thermal diffusivity of silicon ensures rapid thermal equilibration relative to the sample frequency. An accelerometer was placed in the bulk LN_2 to record the g-level, while a pressure transducer monitored the bulk LN_2 pressure (P_{sat}). A resistive temperature detector (RTD) was fixed in the chamber to measure bulk liquid temperature. The chamber was fitted with a relief valve for pressure control.

During ground tests, the chamber was vented to laboratory atmosphere (~101 kPa), while the relief valve was used to prevent over-pressurization during the flight. All sensors were connected to a National Instruments data acquisition (DAQ) system controlled via LabVIEW, enabling automated experiment control and data logging. A DC power supply (Kepco: KLP 600-4) supplied the heating power in constant-voltage mode. Heater voltage and current were logged using two multimeters, i.e., one connected in series for current measurement and the other in parallel for voltage measurement. The instantaneous heat flux (q'') was calculated using the measured voltage (V) and current (I) inputs to the thin-film heater, normalized by the heating area (A_{h}) as $q'' = (V \cdot I)/A_{\mathrm{h}}$. The boiling surface temperature (T_{w}) was determined by accounting for the temperature drop across the 500 μm silicon substrate and the 1 μm SiO_2 layer. Although the SiO_2 layer is only 1 μm, its low thermal conductivity ($k_{\mathrm{SiO_2}} \approx 0.54\ \mathrm{W/(m \cdot K)}$) relative to silicon ($k_{\mathrm{Si}} \approx 1360\ \mathrm{W/(m \cdot K)}$) makes it the dominant thermal resistance in the conduction path[24,25]. The high cryogenic thermal conductivity of silicon is consistent with prior measurements and reflects the expected increase in lattice thermal conductivity of crystalline materials at low temperature[25]. Assuming one-dimensional steady-state heat conduction, the surface temperature was estimated as $T_{\mathrm{w}} = T_{\mathrm{b}} - q''\left(\frac{t_{\mathrm{Si}}}{k_{\mathrm{Si}}} + \frac{t_{\mathrm{SiO_2}}}{k_{\mathrm{SiO_2}}}\right)$, where T_{b} is the base temperature, t is the layer thickness, and k is the thermal conductivity at the LN_2 saturation temperature. Consequently, the wall superheat (ΔT_{w}) was defined as the difference between the calculated wall temperature and the fluid saturation temperature: $\Delta T_{\mathrm{w}} = T_{\mathrm{w}} - T_{\mathrm{sat}}$. While our initial bounding estimate indicated a minimal through-thickness temperature drop (≈ 0.06 K across the silicon and ≈ 0.30 K across the oxide), we have further justified this assumption through 3D numerical simulations (ANSYS) that quantify lateral heat spreading and thermal constriction. The model applied a uniform heat flux over the heater footprint, an effective convective boundary condition at the boiling interface, and adiabatic conditions on the insulated lateral and back surfaces, consistent with the experimental thermal insulation. The analysis showed that thermal spreading introduces only a minor correction to the estimated wall temperature and heat flux which ensures that any potential error introduced by the 1D assumption is rigorously bounded and does not bias the reported boiling trends. A detailed uncertainty analysis is provided in Supplementary Note 5 of the Supplementary Information. The saturation temperature (T_{sat}) of the liquid nitrogen was monitored continuously during the experiments using the RTD immersed in the bulk LN_2.

Parabolic flight

Reduced gravity conditions for the pool boiling experiments were achieved using a parabolic flight campaign operated by Zero-G, in which an aircraft executes a series of parabolic maneuvers to simulate microgravity. Each parabola consists of a roughly 65–70 second maneuver, including an approximately 20-second microgravity windows (0±0.02 g) bracketed by hypergravity periods (≈1.8 g) during the pull-up and pull-out phases (Figure 3a). Here, a/g is the aircraft acceleration (a) normalized with gravitational acceleration (g). These repeated trajectories provided consistent access to reduced gravity conditions. Figure 3b presents the time-resolved acceleration data from a representative parabola. The data clearly show a sharp transition from the hypergravity phase (≈1.8 g) to the near-zero gravity test period. Minor acceleration fluctuations, or g-jitter, were observed throughout the 20-second low-g period, typically remaining less than ±0.02 g (Further details are provided in Supplementary Note 3 and Supplementary Figure 4).

Figure 3c shows the complete time history of acceleration data for the entire flight session. The repeated parabolic maneuvers are visible as sharp, periodic drops in acceleration, with each drop corresponding to a microgravity interval. This consistent and repeatable pattern was leveraged to incrementally approach the CHF over three consecutive low-g parabolas, allowing multiple measurements to confirm the repeatability. Since the LN_2 tank was vented to the ambient pressure outside the aircraft, the fluid saturation pressure and temperature varied with changes in the aircraft's altitude during the parabolic cycles. Figure 3d illustrates the corresponding change in the LN_2 saturation pressure (P_{sat}) and saturation temperature (T_{sat}) over the course of the parabolic flight. This measured saturation temperature is used for calculating the wall superheat (ΔT_{w}). To ensure that the measurements reflect steady-state microgravity boiling rather than transition transients, data acquisition was triggered only after the system had fully entered the microgravity regime. This timing ensures that the gravity level remained stable throughout the measurement window. During each low-g period, the heater power was ramped at a controlled rate to generate the boiling curve data. Although the heater power was continuously increased during the microgravity window, the thermal response time of the test section is substantially shorter than the 20 s reduced-gravity interval. Based on characteristic thermal diffusion timescales, thermal equilibration across the 500 μm silicon substrate and 1 μm SiO_2 layer occurs on sub-millisecond timescales, more than four orders of magnitude shorter than the ≈20 s reduced-gravity interval. Consequently, the substrate thermal response introduces no significant transient bias. The wall temperature tracks the imposed heat flux essentially instantaneously, and the boiling process evolves through a sequence of quasi-steady states during the power ramp. This allows ONB, HTC, and CHF to be extracted as quasi-steady quantities.

Results

Terrestrial (1-g) boiling characterization

We first characterized the pool boiling heat transfer of liquid nitrogen (LN_2) under terrestrial gravity (1-g) to establish a rigorous baseline. Figure 4a plots the boiling curve, i.e., heat flux (q'') versus wall superheat (ΔT_{w}), alongside literature data for metallic surfaces[13,15]. The ONB superheat was identified as the first inflection point where the slope abruptly deviates from the natural convection regime. Beyond ONB, the surface entered the nucleate boiling regime, with HTC values ranging from 4.4×10^3 to 23.7×10^3 W/(m^2·K). As the heat flux approached the CHF of 16.15 W/cm^2, the wall temperature exhibited characteristic instability. The CHF was defined phenomenologically as the point of transition from nucleate boiling to the film boiling regime. In our experiments, this transition was characterized by a simultaneous wall temperature excursion and a sharp decrease in heater current. The reported CHF value corresponds to the highest stable heat flux attained immediately prior to this instability. To prevent permanent thermal damage to the microfabricated heater and integrated sensors, power was terminated immediately upon the detection of this dual signature[26,27].

A comparison with literature data reveals significant discrepancies between the metallic surfaces. The copper surface data from Edeskuty et al[13]., for example, exhibits a significantly higher ONB and lower HTC compared to the copper data from Bombardieri et al[15]. This variance within the same material underscores that surfaces based on metallic substrates are unreliable baselines, as their performance is dictated by uncontrolled surface defects (scratches, cavities) rather than intrinsic material properties. Compared to all metallic references, our ultra-smooth SiO_2 surface exhibited a consistently higher ONB superheat. This is physically consistent with the classical nucleation theory; that is, the lack of micro-cavities necessitates higher wall superheats to activate nucleation sites. Furthermore, our measured CHF aligns well with literature benchmarks, confirming that while ONB and HTC are highly sensitive to surface topography, the transition to the boiling crisis is less sensitive to intrinsic microscale defects[21,28,29].

Reduced gravity (μ-g) boiling dynamics

Following the terrestrial baseline, we conducted LN_2 boiling tests under reduced gravity aboard a parabolic flight. To ensure statistical reliability, μ-g boiling data were collected across nine separate parabolic maneuvers, resulting in three independent boiling curves (Figure 4b). The high degree of overlap between these curves indicates that the measured boiling behavior is not dominated by transient disturbances or g-jitter. Quantitatively, the ONB wall superheat extracted from the three independent reduced-gravity boiling curves was 4.73 ± 0.23 K, and the CHF was 5.19 ± 0.40 W/cm². To further evaluate repeatability, HTC was calculated at three characteristic boiling states: ONB, mid-nucleate boiling ($q" \approx 4$ W/cm²), and near CHF ($q" \approx 5$ W/cm²). The corresponding HTC values were $2.58 \pm 0.55 \times 10^3$, $6.12 \pm 0.50 \times 10^3$, and $8.56 \pm 0.33 \times 10^3$ W/(m²·K), respectively. The repeatability observed across independent parabolic maneuvers further supports that the extracted ONB, HTC, and CHF values are representative of quasi-steady boiling behavior rather than transient thermal excursions. The slight lateral shifts are attributed to minor variations in fluid saturation temperature (from 72.1 to 73.1 K) during flight maneuvers. Because the ground and parabolic-flight experiments were conducted at different operating pressures, all boiling curves were reduced using wall superheat, $\Delta T_{\mathrm{w}} = T_{\mathrm{w}} - T_{\mathrm{sat}}$, rather than absolute wall temperature. Therefore, the lower saturation temperature during flight was directly accounted for in the data reduction. Of the difference in absolute ONB temperature between the two conditions, ~5.3 K corresponds to this saturation-temperature shift, while a residual ~1.3 K reflects a genuine reduction in ONB superheat under reduced gravity. Thus, this residual is not a pressure artifact. From the ONB superheat-cavity radius relation, i.e., $\Delta T_{\mathrm{ONB}} = \frac{2\sigma T_{\mathrm{sat}}}{r_{\mathrm{c}} \rho_{\mathrm{v}} h_{\mathrm{fg}}}$, the lower flight pressure reduces the vapor density and would therefore raise the required incipience superheat (with minimal increase in surface tension and roughly flat latent heat with the decrease in pressure), opposite to the observed earlier onset. The earlier nucleation in the reduced gravity is, therefore, consistent instead with buoyancy-suppressed thickening of the near-wall thermal boundary layer[22]. Nevertheless, pressure-dependent variations in LN_2 thermophysical properties may contribute to quantitative differences between the 1-g and reduced-gravity boiling curves. Furthermore, the SiO_2 interface showed no evidence of progressive surface evolution or aging (Supplementary Figure 2); the ONB and CHF values remained stable throughout the flight campaign, confirming that the observed heat transfer characteristics are intrinsic to the reduced-gravity environment. In all cases, the ONB superheat appeared to be around 5 K, and the CHF reached approximately 5−6 W/cm^2. The slight path-dependent shift observed in the reduced-gravity boiling curves is associated with the controlled power-ramp procedure and delayed vapor removal under reduced gravity, rather than a measured hysteresis loop; each curve was acquired during a single, monotonically increasing power ramp. Because buoyant bubble departure is suppressed, residual vapor structures can persist near the heater surface and influence subsequent nucleation and heat-transfer states during the same ramp. This shift is small relative to the gravity-dependent changes reported here and falls within the run-to-run uncertainty, as evidenced by the close overlap of the three independent curves (Figure 4b). This decrease in CHF is the expected consequence of suppressed buoyancy; without buoyant removal forces, bubble residence time increases, leading to rapid coalescence and premature vapor blanketing. Despite the reduction in CHF, a counter-intuitive enhancement in HTC was observed in the nucleate boiling regime. As shown in Figure 4c, the μ-g boiling curve lies above the 1-g curve prior to CHF, indicating a higher HTC for a given superheat. Consistent with this earlier onset, in the wall superheat 4–6 K range the reduced gravity surface is already in nucleate boiling while the 1-g surface remains in natural convection (Figure 4c). The observed enhancement may therefore reflect both the earlier transition to nucleate boiling and the extended microlayer evaporation discussed above. Contrary to the classical assumption that buoyancy is required for efficient heat removal, our results suggest that heat transfer efficiency can actually be improved in reduced gravity due to suppressed bubble departure. In the absence of strong buoyant forces, vapor bubbles do not detach rapidly; instead, they grow to significantly larger diameters and maintain prolonged contact with the heater surface. This enlarged bubble footprint creates an extended liquid microlayer, i.e., the micron-thin, highly evaporative fluid film trapped between the vapor and the solid wall (Figure 5)[30]. Because this microlayer offers minimal thermal resistance, the substantial increase in its surface area compensates for the low bubble departure frequency, driving the observed enhancement in HTC. The observed enhancement of HTC in reduced gravity is consistent with previous investigations utilizing non-cryogenic fluids, such as R-113 and FC-72 [8,11], which reported that microgravity HTC can be comparable to or even exceed terrestrial values. In addition to extended microlayer evaporation, increased effective nucleation activity may also contribute to the enhanced HTC under reduced gravity. Prior modelling of bubble nucleation on ideally smooth heated surfaces showed that thermal-boundary-layer effects can reduce the superheat required for bubble inception[22]. Orientation-dependent pool boiling experiments further showed that thicker thermal-boundary-layer development can increase nucleation site density[31]. Under reduced gravity, suppressed buoyant departure and delayed vapor removal may similarly modify the near-wall thermal boundary layer, promoting earlier nucleation or increased effective nucleation activity. Therefore, the enhanced HTC observed here is interpreted as a physically plausible outcome of reduced-gravity bubble dynamics, potentially involving both extended microlayer evaporation and increased nucleation activity. Notably, in our work, this validation was achieved using LN_2 on an ultra-smooth heater surface, effectively minimizing the influence of surface-defect interactions on the observed gravity-dependent boiling behavior. By minimizing the influence of surface morphology, we demonstrate that the enhanced HTC is an intrinsic response to the reduced gravity environment, independent of surface conditions.

As noted in previous literature, surface tension and evaporation momentum dominate in microgravity[11,19,32]. In this regime, the enlarged bubble base and extended microlayer evaporation partially compensate for the loss of convective mixing. This benefit, however, is transient; as heat flux increases, excessive bubble coalescence leads to microlayer depletion and dry-patch growth that promote the premature CHF. It is important to note that while we focus on topography, boiling is also influenced by molecular-scale surface states, such as dangling bonds or hydroxyl groups on the SiO_2 interface. However, because these intermolecular interactions are independent of gravitational acceleration, and all our surfaces underwent identical preparation for both 1-g and μ-g testing, these effects do not account for the observed gravity-dependent shifts. Nevertheless, molecular-scale surface interactions cannot be completely eliminated and may still influence the absolute boiling characteristics of the interface. Furthermore, while lateral correlations between surface features can influence liquid spreading and microlayer development[33], the nanoscale smoothness of our substrate ensures that such effects remain negligible relative to the critical scales predicted by classical nucleation theory for liquid nitrogen. This distinguishes our atomically smooth baseline from the relatively smooth metallic surfaces used in prior studies[34], where inherent grain boundaries, oxide patches, and inevitable scratches may still introduce confounding structural variables.

The power of this decoupled baseline becomes evident when comparing our results with the copper surface data from Edeskuty et al.[13] (Figure 4c). Under 1-g, the boiling curves for the smooth SiO_2 and Edeskuty's copper are relatively similar, as strong buoyancy forces dominate bubble detachment, effectively masking subtle differences in surface topography. Under μ-g, however, the prolonged residence time and expanded base of the large bubbles allow the liquid microlayer to spread over a vast area, activating numerous dormant cavities that would otherwise remain inactive. This bubble growth-induced activation may significantly increase the effective nucleation site density on the copper surface. In contrast, our ultra-smooth SiO_2 surface lacks these cavities; therefore, the spreading microlayer cannot trigger secondary nucleation. Considering that enhancing boiling in 1-g typically requires sophisticated microstructure engineering[7,35,36], whereas simple surface defects are sufficient to improve performance in μ-g, this comparison reveals a critical insight: the influence of surface topography is significantly more prominent in microgravity than in terrestrial gravity[1,6]. The absence of buoyancy allows surface features to dictate nucleation dynamics that are otherwise washed out by convective forces in 1-g. Consequently, previous studies[13,15] relying on metallic baselines have likely overestimated the intrinsic effects of microgravity by conflating them with micro-cavity enhancement. This establishes our SiO_2 dataset as a true, well-characterized baseline with minimized topographical effects, highlighting the immense potential of surface topology engineering for targeted boiling enhancement in space systems.

Discussion

In this work, we isolated the dominant influence of surface topography from that of gravitational acceleration, to the extent achievable with a chemically homogeneous, ultra-smooth interface, on the pool boiling characteristics of liquid nitrogen. By utilizing an ultra-smooth silicon dioxide surface, we established a rigorous reference dataset that minimizes the influence of surface-defect induced nucleation sites inherent to traditional metallic substrates. Our terrestrial experiments demonstrated that while the ultra-smooth surface requires a significantly higher wall superheat to trigger the ONB, the subsequent performance aligns closely with established metallic surface data. This confirmation suggests that under normal gravity, buoyancy-driven bubble dynamics dominates the boiling process, effectively marginalizing the influence of minor surface feature differences. In contrast, experiments conducted under reduced gravity revealed a systematic degradation in boiling behavior. We observed a drastic 65% reduction in CHF compared to the 1-g baseline, a direct consequence of suppressed buoyancy leading to bubble coalescence and premature vapor blanketing. Despite this reduction in CHF, the nucleate boiling regime exhibited a counter-intuitive enhancement in HTC in μ-g. We hypothesize this performance gain is associated with extended microlayer evaporation; the lack of buoyancy allows bubbles to grow to larger diameters and remain stationary, thereby maximizing the surface area of highly evaporative liquid microlayer trapped beneath the bubble. Validating this mechanism on an ultra-smooth surface confirms that the HTC enhancement is an intrinsic response to the reduced gravity environment, independent of surface roughness. Furthermore, a comparison with literature data reveals that metallic surfaces exhibit significantly higher HTC and CHF values in μ-g than our smooth baseline. This discrepancy arises because the enlarged bubbles in reduced gravity activate dormant surface cavities on metallic substrates; that is, a coupled gravity-structure effect absent on the defect-minimized SiO_2 surface. The most significant finding of this work is that the influence of surface topography is markedly more prominent under microgravity than in terrestrial conditions. Considering that enhancing boiling in 1-g typically requires sophisticated microstructure engineering, whereas simple surface defects are sufficient to significantly alter bubble dynamics in μ-g, our results indicate that the absence of strong buoyancy allows even subtle surface features to dictate nucleation behavior. These results underscore the necessity of using ultra-smooth, well-characterized surfaces to establish a true baseline for boiling research. By providing this decoupled dataset, this work offers a critical benchmark for validating two-phase flow models and establishes foundational guidance for the rational design of engineered surfaces for space exploration and high-performance cryogenic applications.

Data availability

The datasets generated and analyzed during the current study are available in Zenodo repository, [https://doi.org/10.5281/zenodo.19792024].

Acknowledgments

Y. Song acknowledges the funding support provided by the Herbert Wertheim College of Engineering at the University of Florida. J. Chung acknowledges the support provided by the Andrew H. Hines, Jr./Progress Energy Endowment Fund in the Department of Mechanical and Aerospace Engineering and funds from the Herbert Wertheim College of Engineering at the University of Florida. All experiments were primarily supported by the Flight Opportunities Program at the National Aeronautics and Space Administration (NASA) under grant award number 80NSSC22K0562.

Author contributions

M.S.R. and P.I. contributed equally to this work. **M.S.R:** Data curation (equal); Formal analysis (equal); Investigation (equal); Methodology (equal); Visualization (equal); Writing – original draft, review & editing (equal). **P.I:** Data curation (equal); Formal analysis (equal); Investigation (equal); Methodology (equal); Writing – review & editing (equal). **J.A:** Investigation (equal); Methodology (equal). **J.C:** Funding acquisition (equal). **J.H:** Funding acquisition (equal); Writing – review & editing (equal). **Y.S:** Conceptualization (equal); Formal analysis (Equal); Investigation (equal); Methodology (equal); Funding acquisition (equal); Project administration (equal); Supervision (equal); Validation (equal); Writing – original draft, review & editing (equal).

Competing interests

All authors state that there are no financial or non-financial conflicts of interest to disclose

Additional information

Additional information supporting this study can be found in supplementary file.

References

1. Di Marco, P. Review of reduced gravity boiling heat transfer: European research. J. Jpn. Soc. Microgravity Appl. 20, 252–263 (2003).
2. Mbaye, M., Raza, M. Q., Sebilleau, J. & Colin, C. Flow boiling in microgravity. J. Phys.: Conf. Ser. 2766, 012124 (2024).
3. Hedayat, A., Hastings, L. J., Bryant, C. & Plachta, D. W. Cryogenic propellant long-term storage with zero boil-off. In Proc. Int. Cryogenic Materials Conf., Madison, WI, USA (2001).
4. Dhir, V. K. Boiling heat transfer. Annu. Rev. Fluid Mech. 30, 365–401 (1998).
5. Siegel, R. Effects of reduced gravity on heat transfer. Adv. Heat Transfer 4, 143–228 (1967).
6. Singh, S. K. & Sharma, D. Review of pool and flow boiling heat transfer enhancement through surface modification. Int. J. Heat Mass Transf. 181, 122020 (2021).
7. Cho, H. J., Preston, D. J., Zhu, Y. & Wang, E. N. Nanoengineered materials for liquid–vapour phase-change heat transfer. Nat. Rev. Mater. 2, 16092 (2016).
8. Kim, J. & Raj, R. Gravity and heater size effects on pool boiling heat transfer. NASA Report NASA/CR—2014-216672, University of Maryland, College Park, MD (2014).
9. Colin, C., Fabre, J., Ducasse, A. & Legendre, D. Nucleate pool boiling in microgravity: Recent progress and future prospects. C. R. Mécanique 345, 21–34 (2017).
10. Garivalis, A. I., Nikolayev, V. S., Beysens, D. A. & Garrabos, Y. Critical heat flux on microstructured surfaces in microgravity and in the presence of electric field. In Proc. TFEC 1013–1016 (2021).

11. Straub, J. Boiling heat transfer and bubble dynamics in microgravity. Adv. Heat Transfer 35, 57–172 (2001).
12. Nukiyama, S. The maximum and minimum values of heat transmitted from metal to boiling water under atmospheric pressure. Int. J. Heat Mass Transf. 27, 959–970 (1984).
13. Edeskuty, F. J., Williamson, K. D., Taylor, J. F. & Mendelssohn, K. Pool boiling heat transfer to liquid helium and liquid nitrogen in a nearly zero gravity environment. Los Alamos Scientific Laboratory, Los Alamos, NM (1973).
14. Hasan, M. M., Lin, C. S., Knoll, R. H., Bentz, M. D. & Meserole, J. S. Nucleate pool boiling in the long-duration low-gravity environment of the Space Shuttle. NASA TM-105973; AIAA Paper 93-0465 (1993).
15. Bombardieri, C. & Manfletti, C. Influence of wall material on nucleate pool boiling of liquid nitrogen. Int. J. Heat Mass Transf. 94, 1–8 (2016).
16. Ahmed, S., Carey, V. P. & Motil, B. Marangoni effects in the boiling of binary fluid mixtures. In Proc. Third Microgravity Fluid Physics Conf. (NASA, 1996).
17. Hartwig, J., Chung, J. N., Dong, J., Wang, H., Darr, S. R., DeVore, S., James, S. & McQuillen, J. Nitrogen flow boiling and chilldown experiments in microgravity using pulse flow and low-thermally conductive coatings. npj Microgravity 8, 33 (2022).
18. Sinha-Ray, S., Yarin, A. L., Pourdeyhimi, B. & Kim, J. Swing-like pool boiling on nano-textured surfaces for microgravity applications. npj Microgravity 3, 17 (2017).
19. Zhang, Q., Wang, X., Zhao, Y., Liu, Z. & Wang, E. N. Bubble nucleation and growth on microstructured surfaces under microgravity. npj Microgravity 10, 13 (2024).
20. Song, Y., Zhang, L., Liu, Z., Preston, D. J. & Wang, E. N. Effects of airborne hydrocarbon adsorption on pool boiling heat transfer. Appl. Phys. Lett. 116, 253702 (2020).
21. Hsu, Y. Y. On the size range of active nucleation cavities on a heating surface. J. Heat Transfer 84, 207–213 (1962).
22. Jo, H., Kim, S., Park, H. & Kim, J. Heterogeneous bubble nucleation on ideally-smooth horizontal heated surfaces. Int. J. Heat Mass Transf. 71, 149–157 (2014).
23. Gallo, M., Tiwari, M. K., Oron, A. & Yarin, A. L. A nanoscale view of the origin of boiling and its dynamics. Nat. Commun. 14, 1045 (2023).

24. Glassbrenner, C. J. & Slack, G. A. Thermal conductivity of silicon and germanium from 3 K to the melting point. Phys. Rev. 134, A1058–A1069 (1964).
25. Touloukian, Y. S., Powell, R. W., Ho, C. Y. & Klemens, P. G. Thermophysical Properties of Matter: The TPRC Data Series, Vol. 2, Thermal Conductivity—Nonmetallic Solids. IFI/Plenum, New York (1970).
26. Song, Y. Mechanistic understanding and enhancing pool boiling heat transfer via surface property and structure design. PhD thesis, Massachusetts Institute of Technology (2021).
27. Mudawar, I. Assessment of high-heat-flux thermal management schemes. IEEE Trans. Compon. Packag. Technol. 24, 122–141 (2001).
28. Zuber, N. On the stability of boiling heat transfer. J. Fluids Eng. 80, 711–714 (1958).
29. Zuber, N. Hydrodynamic aspects of boiling heat transfer. PhD thesis, University of California, Los Angeles (1959).
30. Kim, H. & Buongiorno, J. Detection of liquid–vapor–solid triple contact line in two-phase heat transfer phenomena using high-speed infrared thermometry. Int. J. Multiphase Flow 37, 166–172 (2011).
31. Jung, S. & Kim, H. Effects of surface orientation on nucleate boiling heat transfer in a pool of water under atmospheric pressure. Nucl. Eng. Des. 305, 347–358 (2016)
32. Elele, E., Shen, Y., Tang, J., Lei, Q. & Khusid, B. Single-bubble water boiling under Earth and low gravity. npj Microgravity 4, 21 (2018).
33. Palasantzas, G. Wetting on rough self-affine surfaces. Phys. Rev. E 63, 021602 (2001).
34. Bon, B. & Klausner, J. Pool boiling heat transfer of highly wetting fluids on smooth metallic surfaces. Int. J. Heat Mass Transf. 47, 709–716 (2004).
35. Song, Y., Díaz-Marín, C. D., Zhang, L., Cha, H., Zhao, Y. & Wang, E. N. Three-tier hierarchical structures for extreme pool boiling heat transfer performance. Adv. Mater. 34, e2200899 (2022).
36. Song, Y., Gong, S., Vaartstra, G. & Wang, E. N. Microtube surfaces for the simultaneous enhancement of efficiency and critical heat flux during pool boiling. ACS Appl. Mater. Interfaces 13, 12629–12635 (2021).

Figure legends

Figure 1. Topography and wettability of the SiO_2 heater surface. (a) AFM image of boiling surface, revealing nanoscale smoothness. (b) Dynamic contact angle measurement showing a water droplet sliding at a 26.5° tilt. The low contact angle hysteresis (<10°) confirms the high chemical homogeneity and physical smoothness of the surface.

Figure 2. Schematic of the pool boiling experimental setup used for both ground (1-g) and microgravity (μ-g) conditions.

Figure 3. Parabolic flight profile and saturation temperature-pressure response of the liquid nitrogen system. (a) Altitude profile of a parabolic flight showing the ≈20 s microgravity window. (b) Normalized acceleration, a/g, during a single parabola, showing the ≈0 g period and the associated g-jitter. (c) Normalized acceleration over the entire flight, illustrating the sequence of repeated microgravity intervals. (d) Simultaneous time histories of bulk LN_2 temperature (black curve, left axis) and tank pressure (blue curve, right axis) during the parabolic flight.

Figure 4. Decoupled boiling heat transfer analysis of LN_2 on ultra-smooth SiO_2 versus metallic surfaces. (a) Terrestrial (1-g) pool boiling curves. The wide variance between copper datasets[13,15] highlights the inconsistency of metallic baselines, whereas the SiO_2 surface shows high ONB superheat due to the lack of nucleation cavities. (b) Reduced gravity (μ-g) boiling curves from multiple parabolic trajectories, showing consistent earlier ONB and reduced CHF. (c) Comparison of 1-g and μ-g regimes. While 1-g performance is similar between surfaces, μ-g reveals a strong divergence, indicating that surface topography effects are magnified in reduced gravity. Uncertainty for all points on boiling curves is analyzed and detailed in the Supplementary Note 5.

Figure 5. Mechanism of microlayer-induced enhancement. In μ-g (top), reduced buoyancy leads to larger, stationary bubbles with expanded liquid microlayers. On an ultra-smooth surface, this increases evaporative heat flux; on rough surfaces, this mechanism further couples with surface defects to activate secondary nucleation sites.

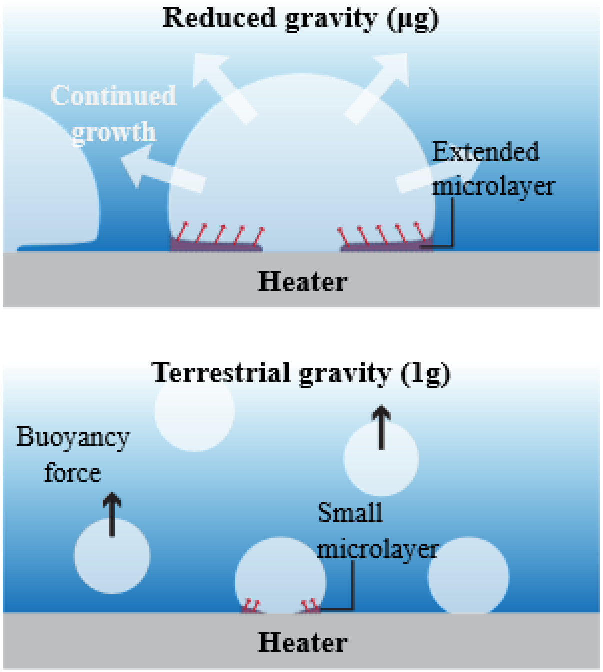

Reduced gravity (μg)
Continued growth
Extended microlayer
Heater
Terrestrial gravity (1g)
Buoyancy force
Small microlayer
Heater

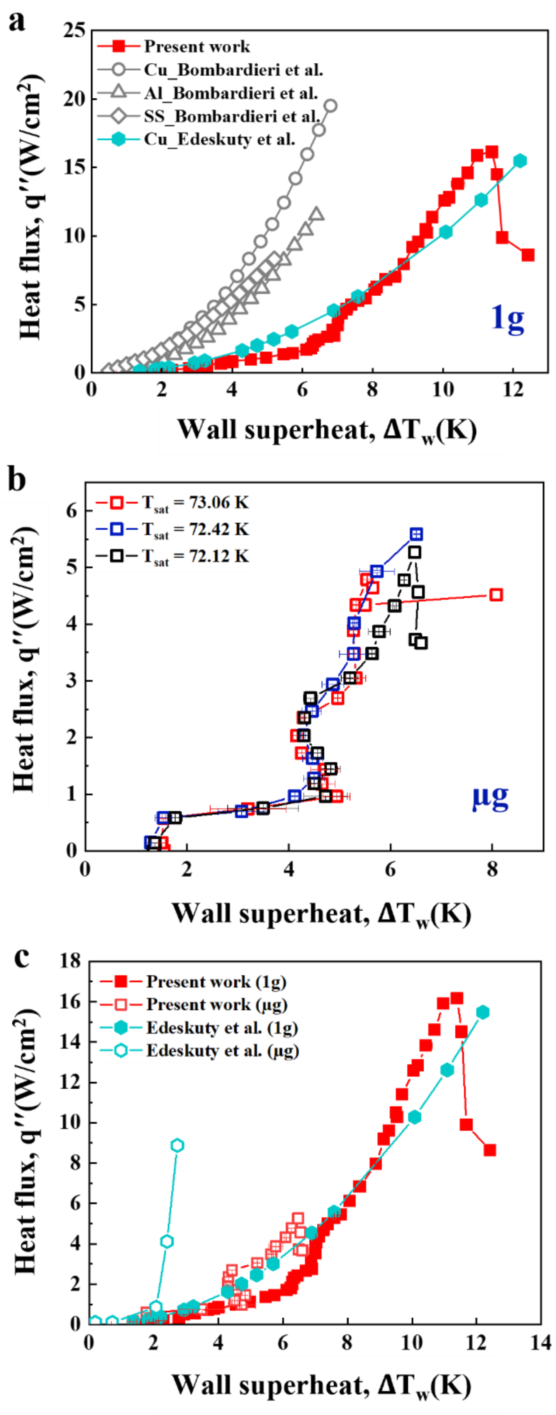
a
Present work
Cu_Bombardieri et al.
Al_Bombardieri et al.
SS_Bombardieri et al.
Cu_Edeskuty et al.
1g
Heat flux, q''(W/cm²)
Wall superheat, ΔTw(K)
b
Tsat = 73.06 K
Tsat = 72.42 K
Tsat = 72.12 K
μg
Heat flux, q''(W/cm²)
Wall superheat, ΔTw(K)
c
Present work (1g)
Present work (μg)
Edeskuty et al. (1g)
Edeskuty et al. (μg)
Heat flux, q''(W/cm²)
Wall superheat, ΔTw(K)

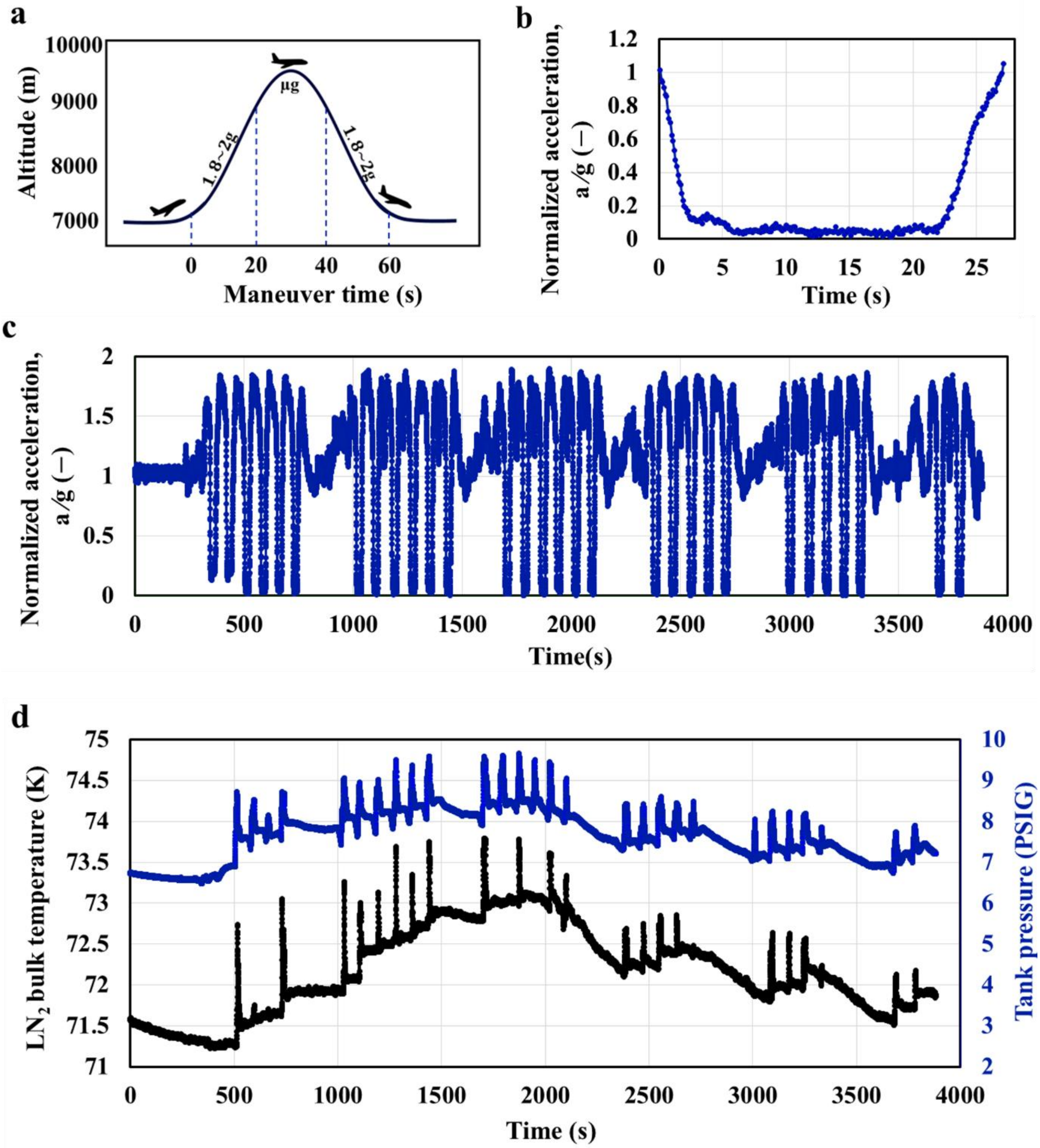
a
Altitude (m)
10000
9000
8000
7000
μg
1.8~2g
1.8~2g
0
20
40
60
Maneuver time (s)
b
Normalized acceleration, a/g (−)
1.2
1
0.8
0.6
0.4
0.2
0
0
5
10
15
20
25
Time (s)
c
Normalized acceleration, a/g (−)
2
1.5
1
0.5
0
0
500
1000
1500
2000
2500
3000
3500
4000
Time(s)
d
LN2 bulk temperature (K)
75
74.5
74
73.5
73
72.5
72
71.5
71
Tank pressure (PSIG)
10
9
8
7
6
5
4
3
2
0
500
1000
1500
2000
2500
3000
3500
4000
Time (s)

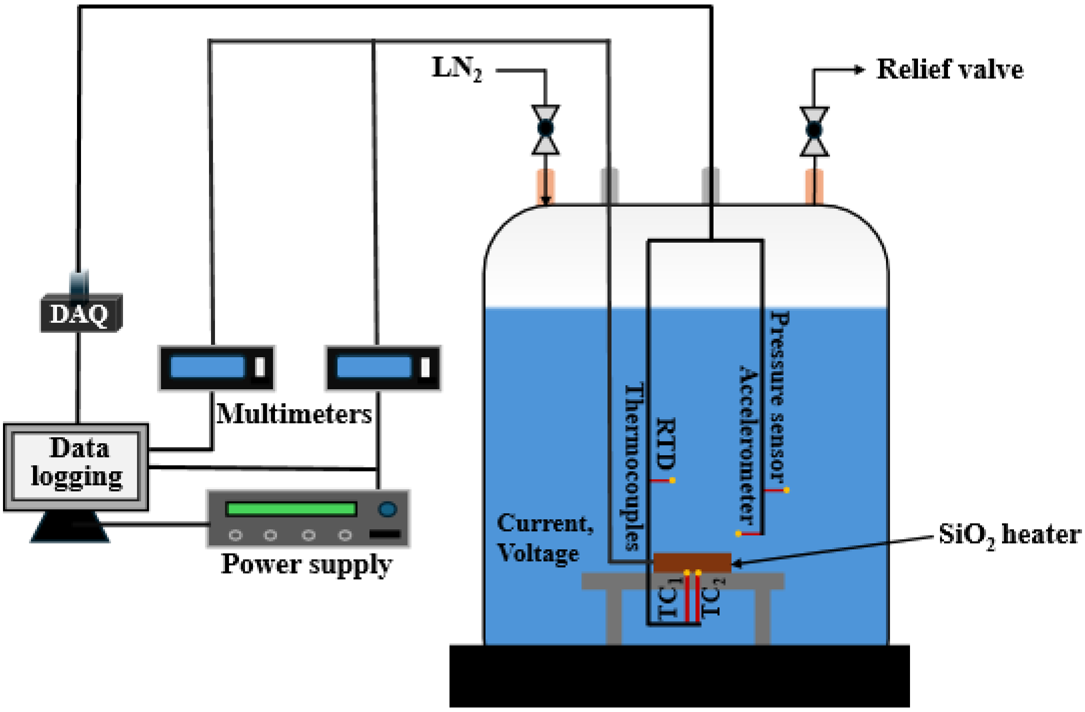

LN2
Relief valve
DAQ
Multimeters
Data logging
Power supply
Current, Voltage
Thermocouples
RTD
Accelerometer
Pressure sensor
SiO2 heater
TC1
TC2

1

a
b
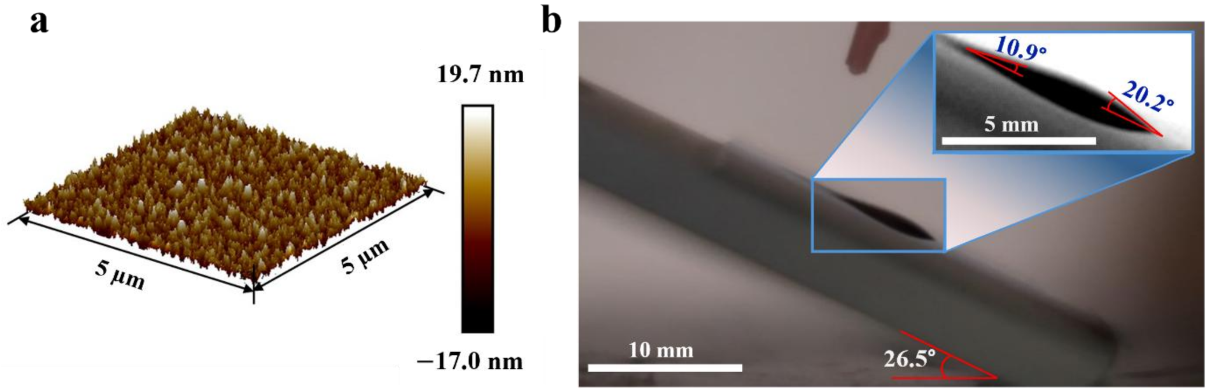

19.7 nm
−17.0 nm
5 µm
5 µm
10.9°
20.2°
5 mm
10 mm
26.5°

2